Energy Equip. Sys./ Vol. 10/No. 4/Dec. 2022/ 439-457

ENERGY EQUIPSYS

Energy Equipment and Systems

http://energyequipsys.ut.ac.ir
www.energyequipsys.com

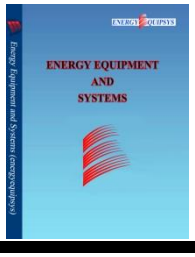

Thermodynamic evaluation of a SOFC-based hybrid system integrated with HDH desalination unit

Authors

Hadi Ghaebi [a*]
Samareh Ahmadi [a]

[a] Department of Mechanical Engineering, Faculty of Engineering, University of Mohaghegh Ardabili, P.O.Box 179, Ardabil, Iran

Article history:

Received : 15 November 2022
Accepted : 27 December 2022

ABSTRACT

A new unified system that runs with solid oxide fuel cells (SOFC) is proposed. Thermodynamic laws have been used to describe and analyze system performance. For this purpose, the reported system is simulated by the EES (Engineering Equations Solver) software. The calculations of this study show that the introduced hybrid system generates net electricity, and distilled water of 460.3 kW, and 307.368 kg/h, correspondingly. Also, the total energy and exergy efficiencies for the whole system are obtained as 81.87 and 55.26, respectively. It was also found that increasing the pressure and using the gas turbine in the fuel cell cycle would increase the SOFC energy and exergy efficiency from values 53.88 and 51.97 to energy and exergy electrical efficiency values of 56.76 and 54.75. Additionally, the heater, afterburner, and SOFC stack are recognized as the utmost destructive constituents by 61.22, 58.75 kW and 5.46 kW, correspondingly. Also, the influence of influential factors on system performance including solid oxide fuel cell current density and its inlet temperature, high desalination temperature, humidifier effectiveness, compression ratio, dehumidifier effectiveness and desalination flow ratio has been studied.

Keywords: Hybrid System; SOFC; HDH System, Thermodynamic, Energetic, Exergetic.

1. Introduction

In recent years, the environmental crisis and the depletion of fuel have led scientists to look for other ways to supply energy. Meantime, economic concerns about fossil fuels have made them more susceptible to obsolescence after the encountered economical recessions in recent decades. This fact leads to more work by scholars to fight against the energy-shortage dilemma by devising high-efficacious strategies. To this end, the use of renewable energy sources, the introduction of multigeneration systems and the improvement of their performance, have been much attention in recent studies. Various renewable-based resources are inspected since then to run various integrated energy plants and augment their extraction scale for the growing populated zones by devising innovative approaches. Among all approachable clean resources, it has been found that fuel cells are the most becoming and available sources on account of the attained recent advances. A solid oxide fuel cell (SOFC) is an electrochemical transformer device that oxidizes fuel to produce electricity at long start-up times and high temperatures. SOFC works with some distinctive features such as low

* Corresponding author: Hadi Ghaebi
Department of Mechanical Engineering, Faculty of Engineering, University of Mohaghegh Ardabili, P.O.Box 179, Ardabil, Iran
Email: hghaebi@uma.ac.ir

emission, low cost, low volume, high efficiency, and fuel flexibility, which makes it a more appropriate selection for integrating with a gas turbine (GT), organic Rankine cycle (ORC), Kalina cycle (KC), and so on. Several studies have addressed this need by integrating SOFC with different electricity generation sub-cycles. For instance, Jia et al. [1] compared three SOFC-based power set-ups namely, simple SOFC, SOFC-GT, and SOFC-GT-ST (steam turbine) units. The findings outlined that the SOFC-GT unit produces near 80% and 60% higher overall and power efficiencies, respectively.

In addition, the heat dissipation of the systems can be used to run the desalination systems for distilled water production. Ghaebi et al. [2] introduced a promising polygeneration system to generate distilled water from HDH (humidification-dehumidification) cycle, electricity, heating, and cooling concurrently from a low-temperature geothermal source. They outlined the operation setting of the introduced system by computing thermodynamic efficiencies and the cost of the operation of the recommended set-up and products, while optimizing the operation of this monolithic system. Their outcomes indicated an optimum energetic efficiency of 94.84%, exergetic efficiency of 47.89%, and OPC of 89.95 $/GJ. The group also evaluated the influence of several central input data on the crucial factors, indicating that the thermodynamic efficiencies could be maximized in terms of freshwater mass flow rate.

Monolithic power plants like hybrid systems play a significant role in providing useful commodities for different uses. Various renewable heat sources are utilized for this target, as described above, where these works in the literature are cited in what follows in terms of SOFC heat source type.

Behzadi et al. [3] proposed a biomass-based solid oxide fuel cell that integrated with a gas turbine, a reverse osmosis desalination unit, and a double-effect absorption chiller to generate power, cooling and fresh water. According to their study, environmental contamination of the proposed system is mitigated by capturing and recycling emitted CO_2 into the gasifier. Also, they performed a parametric study to analyze their proposed multi-generation system from energy, exergy, exergoeconomic, and environmental impact viewpoints.

In another analogous study, Gholamian and Zare [4] took into account the environmental and thermodynamics criteria to juxtapose the running condition of the SOFC/GT, SOFC/GT/ORC, and SOFC/GT/KC systems. The outcomes portrayed that in the case when an ORC or KC is added to a SOFC-GT unit, the energetic and exergetic efficiencies along with net electricity increase. Accordingly, they attained exergetic efficiency of 59.53% and 62.35% for the SOFC/GT/KC and SOFC/GT/ORC units, respectively.

Ranjbar et al. [5] assessed an innovative SOFC-based hybrid set-up, using thermodynamic relations as a tool to achieve a thoroughgoing sensitivity analysis of some central parameters on the trend of the hybrid unit. They reckoned the use of the SOFC/GT unit for electricity, a generator/absorber heat exchanger (GAX) cycle refrigeration, and a recovery heat exchanger (RHX) unit for heating provisions. They improved the energetic efficiency of the unit by up to 33% in collation with the basic set-up. In this evaluation, the fuel cell stack, air heat exchanger, and afterburner were recognized as the source of losses. Then, Chitsaz et al. [6] presented exergoeconomic optimization of the reckoned set-up and calculated unit cost of 26.5-34.2 $/GJ.

A nadir point is seen for the unit cost versus the fuel cell temperature. Later, the influence of the recycling process in the cathode and anode parts on the hybrid set-up operation was inspected by also Chitsaz et al. [7] for the same configuration. They deduced that employing anode recycling ameliorates the operation of the set-up by up to six percent.

Hosseinpour et al.[8] introduced a new cogeneration system consisting of biomass gasification fed by wood, a solid oxide fuel cell and a Goswami cycle, where the Goswami cycle has been used as a supplementary cycle to recover waste heat of the SOFC in order to produce a cooling effect along with additional electricity. They assessed the system in terms of energetic efficiency and exergetic efficiency and the effects of key parameters on the system performance.

Al-Sulaiman et al. [9] presented a thermodynamic simulation of three trigeneration set-ups, utilizing three heat sources of biomass, SOFC, and solar energy, and spotlighted the merits of trigeneration units that are run with SOFC. Based on their conclusion, the SOFC-based energy units have high electrical performance than other sources, whilst are not superior in terms of total performance since they have relatively high CO_2 emission value.

Yari et al. [10] deliberated syngas and biogas to operate two cogeneration systems based on SOFC as a topping unit and juxtaposed their efficiency in terms of cost and thermodynamics. They found that the unit with SOFC and digester outperforms its counterpart when a gasifier is used instead of a digester, while its overall efficiency is not superior. In terms of cost analysis, the inspection clarified that the system with SOFC and digester has nearly 54% lower cost of the product than its counterpart when a gasifier is used instead of a digester.

Hosseini et al. [11] presented a new cogeneration unit with a SOFC as a topping cycle for seawater desalination and electricity extraction. It should be noted that they used a multi-effect desalination (MED) unit, where a humidification-dehumidification unit is utilized. They argued on the substantial impact of SOFC pressure on distilled water and electricity rates.

Sattari Sadat et al[12] proposed a multigeneration system based on a solid oxide fuel cell, which combines a solid oxide fuel cell and gas turbine, a heat recovery heat exchanger, an ejector refrigeration chamber, and a PEM (proton exchange membrane) electrolyzer. They evaluated it on the basis of the first law of thermodynamics as well as parametrically.

In light of the inspected open literature and by scrutinizing many other similar surveys, it can be understood that no examination of the polygeneration set-ups for generating potable water and electricity, based on the SOFC and HDH system is introduced. The introduced system distilled water from the waste heat of the SOFC/GT cycle after the generation of heating, using an HDH system. The preeminent goals of the current study are multi-facet and are:

- To introduce an innovative new set-up for the production of potable water and electricity, operating with a fuel cell as clean energy.
- To examine the plausibility of the introduced set-up from the thermodynamic vantage point.

To posit some amendments to bolster the efficiency of the unit by altering the influential parameters.

Nomenclature

A_a	The surface area of the active zone (m^2)
AB	Afterburner
AC	Air compressor
c_p	Specific heat capacity at constant pressure ($kJ/kg.K$)
c_v	Specific heat capacity at constant volume ($kJ/kg.K$)
CR	Compression ratio
$D_{a,eff}$	Effective gaseous diffusivity through anode (m^2/s)
$D_{c,eff}$	Effective gaseous diffusivity through cathode (m^2/s)
$\dot{E}x$	Exergy rate (kW)
F	Faraday constant (C/mol)
FC	Fuel compressor
G	Gibbs free energy (kJ)
GT	Gas turbine
H	Heater
h	Specific enthalpy (kJ/kg)
HDH	Humidification-dehumidification
I	Current (A)
i	Current density (A/m^2)
i_{as}	Anode-limiting current density (A/m^2)
i_{cs}	Cathode-limiting current density (A/m^2)
i_{0a}	Exchange current density of anode (A/m^2)
i_{0c}	Exchange current density of cathode (A/m^2)
K_{sh}	The equilibrium constant of the shift reaction
L	SOFC layer thickness, (m)
LHV	Lower heating value (kJ/kg)
$\dot{m}$	Mass flow rate (kg/s)
m_r	Desalination flow ratio

$\dot{n}$	Molar rate (mol/s)
N_{cell}	Number of fuel cells
P	Pressure (bar)
$\dot{Q}$	Heat transfer rate (kW)
$\bar{R}_{uni}$	Universal gas constant $(J/mol.K)$
r_{sc}	Steam to carbon ratio
s	Specific entropy $(kJ/kg.K)$
S	Salinity (g/kg)
SOFC	Solid oxide fuel cell
T	Temperature (K)
TTD	Terminal temperature difference (K)
U_f	Fuel utilization factor
V	Voltage (V)
$\dot{W}$	Electricity (kW)
x	The extent of steam reforming reaction for methane (mol/s)
y	The extent of water gas shift reaction (mol/s)
z	The extent of electrochemical reaction (mol/s)

Greek Symbols

ε	Effectiveness
η	Efficiency
ρ	Electrical resistivity of cell components
φ	Relative humidity
ω	Humidity ratio, mass basis (kg-water vapor/kg dry air)

Subscripts and superscripts

a	Air
AC	Air compressor
act	Activation
an	Anode
ap	Approach point
cat	Cathode
ch	Chemical
conc	Concentration
D	Destruction
da	Dry air
Dhu	Dehumidifier
dp	Dew point
dw	Distilled water
elec	Electrical
el	Electrolyte
en	Energetic
ex	Exergetic
F	Fuel
FC	Fuel compressor
GT	Gas turbine
Hu	Humidifier
in	Inlet
is	Isentropic
int	Interconnect
inv	DC to AC inverter
k	k^{th} Component
max	Maximum
min	Minimum
N	Nernst
net	Net value
ohm	Ohmic
out	Outlet
P	Product
ph	Physical
PH	Preheater
s	Constant entropy
sh	Shifting
sofc	Solid oxide fuel cell
sw	Seawater
1, 2, …	Cycle locations
0	Dead state

2. Set-up description and assumptions

Figure 1 outlines the devised hybrid set-up run with an FC module for multi-extraction of potable water and electricity. The set-up is amalgamated from a hybrid SOFC/GT unit and an HDH unit. The descriptive explication of each set-up is oriented in the concerning sub-sections.

2.1. Hybrid SOFC/GT unit description

The SOFC/GT unit encompasses two compartments a SOFC package and a GT cycle. The SOFC package is comprised of an air compressor (AC), a pump, a fuel compressor (FC), three preheaters (PHs), a SOFC stack, a mixer, an inverter, and an afterburner (AB). At first, air at state 1 is compressed by the AC compressor to the SOFC pressure (state 2) and after that, it is preheated before feeding to the module by PH 3

(state 3). Additionally, FC compresses the CH_4 at state 5, while orienting it to PH 2 in order to increase the fuel temperature. H_2O at environment condition is expanded to the pressure of SOFC module by pump 1 and then is led to PH 1 (state 9). The heated H_2O and CH4 are mixed in the mixer and the merged flow is oriented to the stack (state 11). Next, the anode and cathode are replenished by the air and mixture via an electrochemical reaction, correspondingly, to convert DC to AC via an inverter. Surplus air of the unreacted fuel of the anode and cathode combust inside of the AB and is discarded from the exhaust flue at high temperature and pressure. Then high temperature and pressure mixture is oriented back to preheat H_2O, CH_4, and air through the preheaters. After that, the flue gases are expanded through the GT to produce electricity.

2.2.HDH system's description

The exhaust gases of the gas turbine have high temperatures, so they are fed into the HDH system as a heat source for generating distilled water. In this stage, the water with specific salinity is guided to an open loop, while the air stream circulates in a closed circuit. Also, a heater is embedded to heat the seawater before the humidifier. In the humidifier, the salty water goes through an evaporation process with air and the remains are thrown away from the humidifier in the form of brine, while the air is humidified. In the end, humid air cracks the humidifier and enters the dehumidifier, and distilled water is yielded by distilling the moisture in the air.

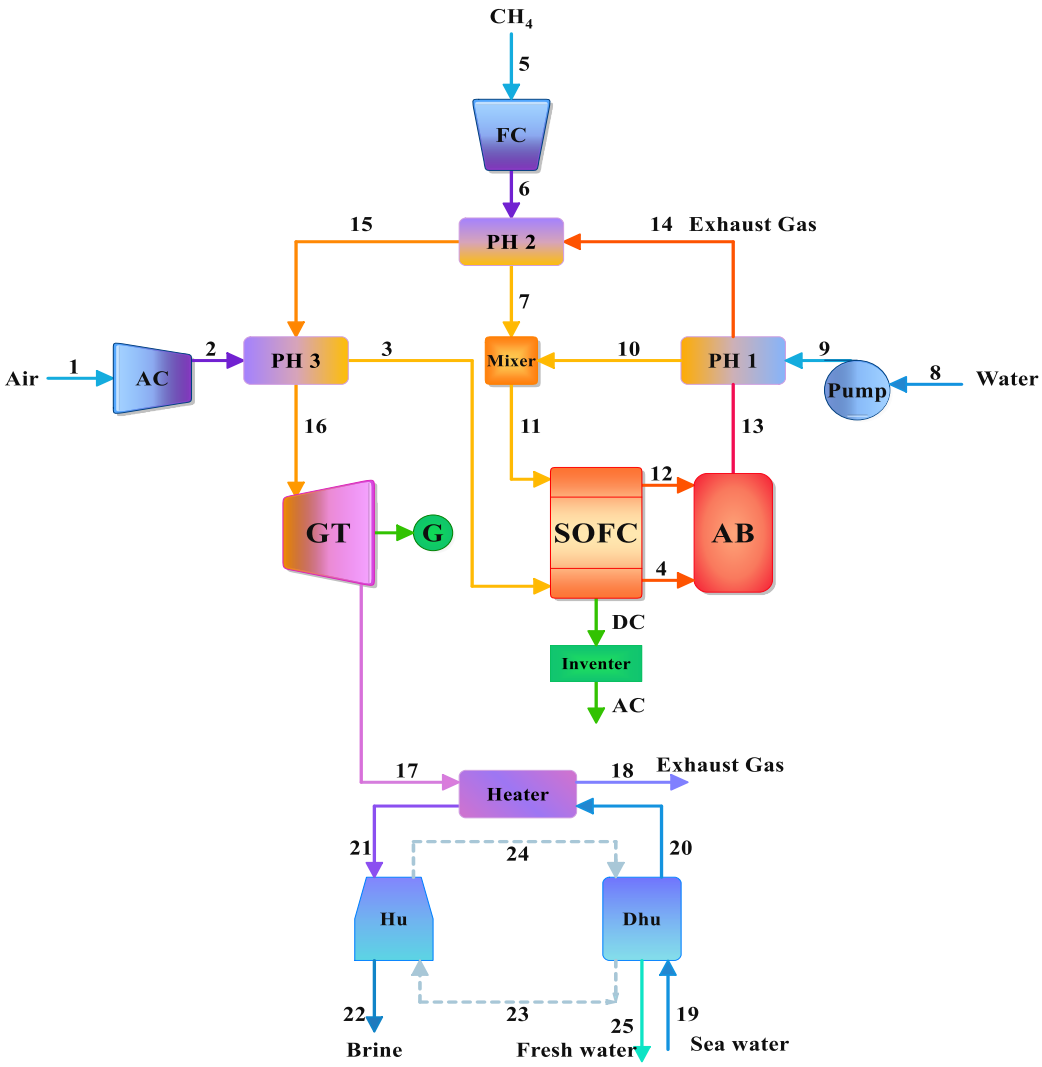

Fig. 1. Schematic of the devised innovative hybrid set-up ran by a SOFC

3.System modeling

In this section, the equations used for simulation and system performance evaluation are presented.

3.1.SOFC formula

Some assumptions are considered for the simulation of the SOFC set-up as follows [5, 13]:

- Air includes around 79 % N_2 and 21 % O_2.
- The SOFC system operates at thermodynamic equilibrium and steady-state (SS) settings.
- The energies of kinetic and potential are constant throughout the hybrid SOFC/GT set-up.
- The cathode and anode pressures are constant and equal.
- In the afterburner, the unreacted gases are utterly oxidized.
- Between solid structure and gas channel heat transfer due to radiation is neglected.
- No gas leaks from the SOFC package.
- Contact resistance is neglected.
- CH_4 amount at the end of reforming is utterly consumed.
- The pressure drop across the SOFC, afterburner, and preheaters are presumed 2%, 3%, and 2%, respectively.

In the present study, internal reforming is used, as it is reported to be a better choice compared to external reforming [13]. Hence, the reaction mechanisms that have occurred within the cathode/anode are articulated below:

Reforming:

$$CH_4 + H_2O = 3H_2 + CO \quad (1)$$

Shifting:

$$CO + H_2O = H_2 + CO_2 \quad (2)$$

Electrochemical:

$$\frac{1}{2}O_2 + H_2 = H_2O \quad (3)$$

It is presumed that the shifting reaction is reached the thermodynamic equilibrium, and hence the equilibrium constant may be articulated as

$$\ln K_{sh} = -\frac{\Delta \bar{g}^{0}_{sh}}{\bar{R}_{uni} T_{sofc}} = \ln\left[\frac{y \times (3x + y - z)}{(x - y) \times (1.5x - y + z)}\right] \quad (4)$$

where T_{sofc} is the SOFC outlet temperature and $\bar{R}_{uni}$ is the universal gas constant. Also, $\Delta \bar{g}^{0}_{sh}$ is the Gibbs free energy at the SOFC temperature, articulated as

$$\Delta \bar{g}^{0}_{sh} = \bar{g}^{0}_{sh,CO_2} + \bar{g}^{0}_{sh,H_2} - \bar{g}^{0}_{sh,H_2O} - \bar{g}^{0}_{sh,CO} \quad (5)$$

$$\bar{g}^{0}_{sh} = \bar{h} - T_{sofc} \cdot \bar{s}^{0} \quad (6)$$

Here, $\bar{s}^{0}$ and $\bar{h}$ are, respectively, the standard entropy and enthalpy per molar.

Assuming that the molar conversion rates for Eqs. (1)-(3) are x, y, and z, respectively, the mass balance between the exit and inlet of the SOFC module is articulated as

$$\dot{n}_{CH_4,in} = x \quad (7)$$

$$\dot{n}_{H_2O,in} = r_{sc} \cdot x \quad (8)$$

$$\dot{n}_{H_2,out} = 3x + y - z \quad (9)$$

$$\dot{n}_{CO,out} = x - y \quad (10)$$

$$\dot{n}_{CO_2,out} = y \quad (11)$$

$$\dot{n}_{H_2O,out} = (r_{sc} - 1)x - y + z \quad (12)$$

$$, z = U_f (3x + y) \quad (13)$$

where U_f is the fuel utilization factor.

The whole process of voltage calculation is depicted in Fig. 2. [14-16].

The current and current density may be articulated correspondingly as

$$I_{sofc} = i \cdot A_a \quad (14)$$

$$i = z \cdot n_e \cdot F / N_{cell} A_a \quad (15)$$

where A_a is the active surface area, and n_e is the number of electrons that participated in the electrochemical reaction (n_e=2).

The SOFC electricity and AC-electrical power of the stack can be articulated correspondingly as

$$\dot{W}_{sofc} = I_{sofc} \cdot N_{cell} \cdot V_{sofc} \quad (16)$$

$$\dot{W}_{sofc,inv} = \eta_{inv} \cdot \dot{W}_{sofc} \quad (17)$$

where N_{cell} is the number of cells and η_{inv} is the DC-AC inverter efficiency.

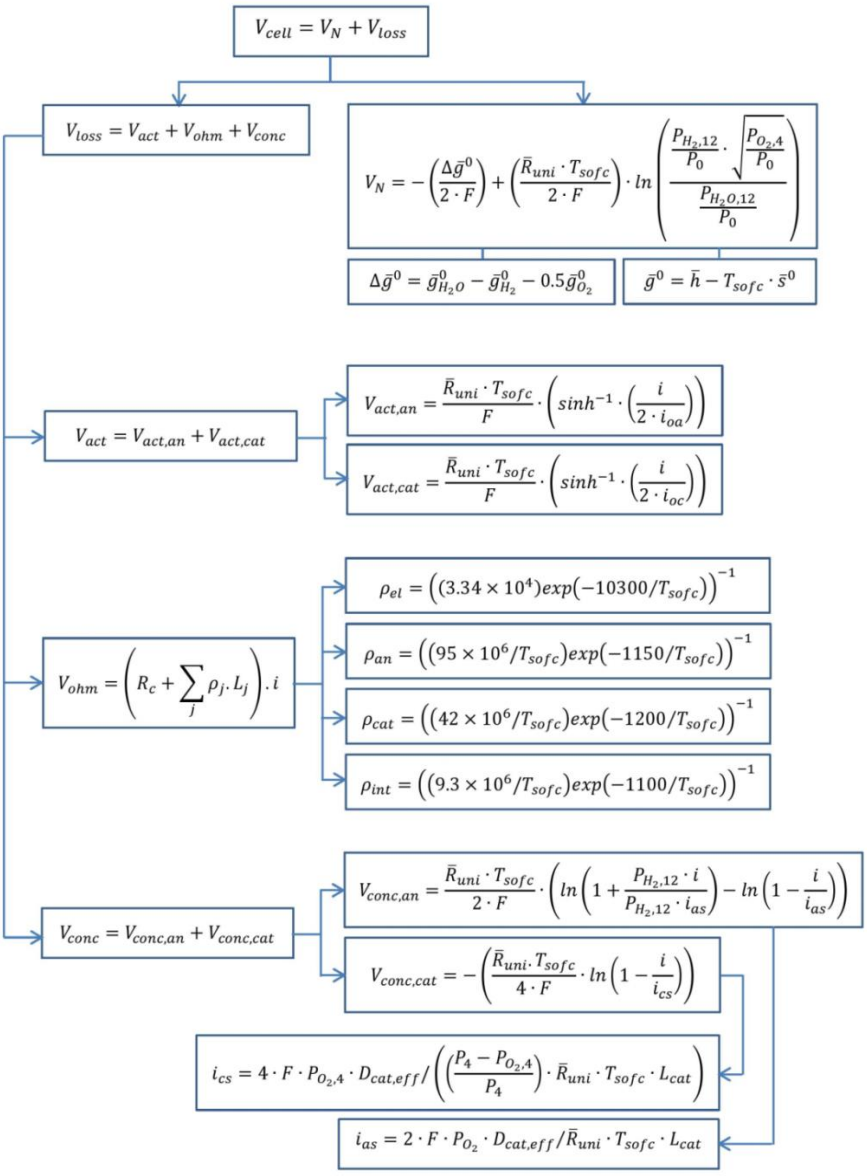

Fig.2. Flowchart of voltage calculation

3.2.HDH formula

The effectiveness of a dehumidifier/humidifier is the ratio of real enthalpy difference to the maximum plausible enthalpy difference:

$$\varepsilon = \frac{\Delta\dot{H}}{\Delta\dot{H}_{max}} \tag{18}$$

The ideal enthalpy for the outlet air is the fully saturated outlet air enthalpy at the inlet water temperature, and when the water temperature is equal to the inlet air dry-bulb temperature, the ideal enthalpy for the outlet seawater is calculated.

The desalination flow ratio is the seawater mass flow rate ($\dot{m}_{sw}$) to the air mass flow rate ($\dot{m}_{da}$) given as

$$m_r = \frac{\dot{m}_{sw}}{\dot{m}_{da}} \tag{19}$$

Gain Output Ratio (GOR) is a parameter for measuring HDH and is defined as the production of distilled water by the latent heat of vaporization to the input heat as shown in Table 2.

3.3.Thermodynamic analysis

Below presumptions are made through the design process:

- Steady-state modeling is reckoned.
- It is assumed that the distilled water at the exit of the dehumidifier has a temperature equal to the average of the exit air dry-bulb temperature and the inlet air dew-point temperature in it [17-19].
- The exiting and entering air relative humidity is set at 90%[17].
- The compressors, turbine, and pumps work with an isentropic efficiency of 85%.
- Only physical and chemical exergies are pondered through exergy assessment [20].

Meantime, some major input data required for simulation in this study are reported in Table 1. The general form of governing equations at steady-state for thermodynamic evaluation of a unit can be articulated as

$$\sum \dot{m}_{in} - \sum \dot{m}_{out} = 0 \tag{20}$$

$$\sum (\dot{m} \cdot h)_{in} - \sum (\dot{m} \cdot h)_{out} + \sum \dot{Q}_{in} - \sum \dot{Q}_{out} + \dot{W} = 0 \tag{21}$$

The input fuel rate to operate the system is calculated as

$$\dot{Q}_{in} = \dot{m}_{CH_4} \cdot LHV_{CH_4} \tag{22}$$

where LHV_{CH_4} stands for the lower heating value of the CH_4.

In terms of the second law of thermodynamics, the balance relation of a unit is articulated as

$$\dot{E}x_{D,k} = \sum_{i=1}^{k} \dot{E}x_{in,i} - \sum_{i=1}^{k} \dot{E}x_{out,i} \tag{23}$$

The overall exergy of the fluid stream is declared as

$$\dot{E}x_k = \dot{E}x_{ph,k} + \dot{E}x_{ch,k} \tag{24}$$

where,

$$\dot{E}x_{ph,k} = \dot{m}\left(h - h_0 - T_0\left(s - s_0\right)\right)_k \tag{25}$$

$$\dot{E}x_{ch,k} = \dot{n}_k \left(\sum_k y_i \overline{ex}_i^{ch,0} + \bar{R} \cdot T_0 \sum_i y_i \ln y_i \right) \tag{26}$$

where, $\overline{ex}_i^{ch,0}$ is the standard chemical exergy found in Refs. [15, 16] and y_i is concentration of the ith constituent.

The exergetic efficiency of the kth element is defined as

$$\eta_{ex,k} = \frac{\dot{E}x_{out}}{\dot{E}x_{in}} = \frac{\dot{E}x_{P,k}}{\dot{E}x_{F,k}} \tag{27}$$

3.4.Main performance criteria

The energetic efficiency of the SOFC stack is articulated as

$$\eta_{en,sofc} = \frac{\dot{W}_{sofc,inv}}{LHV_{CH_4}\dot{m}_{CH_4}} \tag{28}$$

The electrical energetic efficiency of the overall set-up is articulated as:

$$\eta_{en,elec} = \frac{\dot{W}_{net}}{LHV_{CH_4}\dot{m}_{CH_4}} \tag{29}$$

where $\dot{W}_{net}$ is the net extracted electricity calculated as

$$\dot{W}_{net} = \dot{W}_{sofc,inv} + \dot{W}_{GT} - \dot{W}_{AC} - \dot{W}_{FC} - \dot{W}_{Pump} \tag{30}$$

The energetic efficiency of the introduced hybrid set-up ran by the fuel cell to generate distilled water, and electricity is articulated as

$$\eta_{en,tot} = \frac{\dot{W}_{net} + \dot{m}_{25} h_{fg,H_2O}}{LHV_{CH_4}\dot{m}_{CH_4}} \tag{31}$$

The exergetic efficiency of the SOFC stack is declared as:

$$\eta_{ex,sofc} = \frac{\dot{W}_{sofc,inv}}{\dot{n}_5 \cdot \overline{ex}_5^{CH_4}} \tag{32}$$

The electrical exergetic efficiency of the overall set-up is declared as:

$$\eta_{ex,elec} = \frac{\dot{W}_{net}}{\dot{n}_5 \cdot \overline{ex}_5^{CH_4}} \tag{33}$$

The overall exergetic efficiency of the devised hybrid set-up is declared as:

$$\eta_{ex,tot} = \frac{\dot{W}_{net} + \dot{E}x_{25}}{\dot{n}_5 \cdot \overline{ex}_5^{CH_4}} \tag{34}$$

Some mass-, energy-, and exergy-based balance relations to each constituent of the reckoned set-up are enumerated in Table 2.

Table 1 Some paramount thermodynamic input data for analysis of the introduced cogeneration system.

Input data	Reference	Value
SOFC		
The reference temperature, T_0 (K)	[5]	298.15
Reference pressure, P_0 (bar)	[5]	1.013
SOFC inlet temperature, T_{sofc} (K)	[21]	860
Compression ratio, CR	[21]	8
The temperature difference between SOFC, ΔT_{sofc} (K)	[21]	100
Active surface area, A_a (m^2)	[22]	0.01
Basis current density, i ($A.m^{-2}$)	[5]	5500
DC–AC inverter efficiency, η_{inv} (%)	-	95
Exchange current density of anode, i_{oa} ($A.m^{-2}$)	[22]	6500
Exchange current density of cathode, i_{oc} ($A.m^{-2}$)	[22]	2500
Anode effective gaseous diffusivity, $D_{a,eff}$ ($m^2.s^{-1}$)	[22]	0.2×10^{-4}
Cathode effective gaseous diffusivity, $D_{c,eff}$ ($m^2.s^{-1}$)	[22]	0.05×10^{-4}
Afterburner combustion efficiency, η_{AB} (%)	-	95
Lower heating value of CH_4, LHV_{CH_4} (kJ/kg)	-	50000
The lower heating value of CO, LHV_{CO} (kJ/kg)	-	10100
Lower heating value of H_2, LHV_{H_2} (kJ/kg)	-	119960
Fuel utilization factor, U_f	[7]	0.8
The thickness of the anode, L_{an} (cm)	[5]	0.05
The thickness of the cathode, L_{cat} (cm)	[5]	0.005
The thickness of electrolyte, L_{el} (cm)	[5]	0.001
The thickness of interconnect, L_{int} (cm)	[5]	0.3
Isentropic efficiency of fuel compressor, air compressor, and pumps, $\eta_{is,FC,Ac\&Pump1,2}$ (%)	[5]	85
Gas turbine isentropic efficiency, η_{GT} (%)	-	85
Number of cells, N_{cell}	[21]	11000
Steam to carbon ratio, r_{sc}	[21]	2
Faraday constant, F (C/mol)	[5]	96,485
HDH		
Bottom temperature, $T_{min,HDH}$ (K)	[21]	298.15
Top temperature, $T_{max,HDH}$ (K)	[21]	348.15
Humidifier and dehumidifier effectiveness, ε_{Hu} & ε_{Dhu}	[23]	0.85
Desalination flow ratio, m_r	-	2.4
Terminal temperature difference, *TTD* (K)	-	60

Table 2 Exergy, energy, and mass balance equations for different components of the devised set-up.

Component	Mass balance Equation	Energy balance Equation	Exergy balance Equation
Air compressor	$\dot{m}_1 = \dot{m}_2$	$\dot{W}_{AC} = \dot{m}_1 (h_2 - h_1)$ $\frac{T_{s,2}}{T_1} = \left(\frac{P_2}{P_1}\right)^{\frac{k_{air}-1}{k_{air}}}$ $\eta_{is,AC} = \frac{T_{s,2} - T_1}{T_2 - T_1}$	$\dot{E}x_{D,AC} = \dot{W}_{AC} - (\dot{E}x_2 - \dot{E}x_1)$
Fuel compressor	$\dot{m}_5 = \dot{m}_6$	$\dot{W}_{FC} = \dot{m}_5 (h_6 - h_5)$ $\frac{T_{s,6}}{T_5} = \left(\frac{P_6}{P_5}\right)^{\frac{k_{CH_4}-1}{k_{CH_4}}}$ $\eta_{is,FC} = \frac{T_{s,6} - T_5}{T_6 - T_5}$	$\dot{E}x_{D,FC} = \dot{W}_{FC} - (\dot{E}x_6 - \dot{E}x_5)$
Pump	$\dot{m}_8 = \dot{m}_9$	$\dot{W}_{Pump} = \dot{m}_8 (h_9 - h_8)$ $\eta_{is,Pump} = \frac{T_{s,9} - T_8}{T_9 - T_8}$	$\dot{E}x_{D,Pump} = \dot{W}_{Pump} - (\dot{E}x_9 - \dot{E}x_8)$
Preheater 1	$\dot{m}_9 = \dot{m}_{10}$ $\dot{m}_{13} = \dot{m}_{14}$	$\dot{Q}_{PH1} = \dot{m}_9 (h_{10} - h_9) = \dot{m}_{13} (h_{13} - h_{14})$	$\dot{E}x_{D,PH1} = (\dot{E}x_{13} - \dot{E}x_{14}) - (\dot{E}x_{10} - \dot{E}x_9)$
Preheater 2	$\dot{m}_6 = \dot{m}_7$ $\dot{m}_{14} = \dot{m}_{15}$	$\dot{Q}_{PH2} = \dot{m}_6 (h_7 - h_6) = \dot{m}_{14} (h_{14} - h_{15})$	$\dot{E}x_{D,PH2} = (\dot{E}x_{14} - \dot{E}x_{15}) - (\dot{E}x_7 - \dot{E}x_6)$
Preheater 3	$\dot{m}_2 = \dot{m}_3$ $\dot{m}_{15} = \dot{m}_{16}$	$\dot{Q}_{PH3} = \dot{m}_2 (h_3 - h_2) = \dot{m}_{15} (h_{15} - h_{16})$	$\dot{E}x_{D,PH3} = (\dot{E}x_{15} - \dot{E}x_{16}) - (\dot{E}x_3 - \dot{E}x_2)$
Mixer	$\dot{m}_{11} = \dot{m}_{10} + \dot{m}_9$	$\dot{m}_{11} h_{11} = \dot{m}_9 h_9 + \dot{m}_{10} h_{10}$	$\dot{E}x_{D,Mixer} = \dot{E}x_7 + \dot{E}x_{10} - \dot{E}x_{11}$
SOFC	$\dot{m}_3 + \dot{m}_{11} = \dot{m}_4 + \dot{m}_{12}$	$\dot{m}_3 h_3 + \dot{m}_{11} h_{11} = \dot{m}_4 h_4 + \dot{m}_{12} h_{12} + \dot{W}_{sofc,inv}$	$\dot{E}x_{D,sofc} =$ $(\dot{E}x_3 + \dot{E}x_{11} - \dot{E}x_4 - \dot{E}x_{12}) - \dot{W}_{sofc,inv}$
Afterburner	$\dot{m}_{13} = \dot{m}_{12} + \dot{m}_4$	$\dot{m}_4 h_4 + \dot{m}_{12} h_{12} = \dot{m}_{13} h_{13} + \dot{Q}_{loss,AB}$ $\dot{Q}_{loss,AB} = (\dot{m}_{H_2,12} \cdot LHV_{H_2,12}) \cdot (1 - \eta_{AB}) +$ $(\dot{m}_{CO,12} \cdot LHV_{CO,12}) \cdot (1 - \eta_{AB})$	$\dot{E}x_{D,AB} = (\dot{E}x_4 + \dot{E}x_{12}) - \dot{E}x_{13}$
Gas turbine	$\dot{m}_{16} = \dot{m}_{17}$	$\dot{W}_{GT} = \dot{m}_{16} (h_{16} - h_{17})$ $\eta_{is,GT} = \frac{h_{16} - h_{17}}{h_{16} - h_{s,17}}$	$\dot{E}x_{D,GT} = (\dot{E}x_{16} + \dot{E}x_{17}) - \dot{W}_{GT}$
Heater	$\dot{m}_{17} = \dot{m}_{18}$ $\dot{m}_{20} = \dot{m}_{21}$	$\dot{Q}_{Heater} = \dot{m}_{17} (h_{17} - h_{18}) = \dot{m}_{20} (h_{21} - h_{20})$ $TTD = T_{18} - T_{20}$ $GOR = \frac{\dot{m}_{dw} \cdot h_{fg}}{\dot{Q}_{Heater}}$	$\dot{E}x_{D,Heater} = (\dot{E}x_{17} - \dot{E}x_{18}) - (\dot{E}x_{21} - \dot{E}x_{20})$
Humidifier	$\dot{m}_{22} = \dot{m}_{21} - \dot{m}_{25}$	$\dot{m}_{22} h_{22} + \dot{m}_{24} h_{24} = \dot{m}_{21} h_{21} + \dot{m}_{23} h_{23}$ $\varepsilon_{Hu} = \max\left(\frac{(h_{24} - h_{23})}{(h_{24,ideal} - h_{23})}, \frac{(h_{21} - h_{22})}{(h_{21} - h_{22,ideal})}\right)$	$\dot{E}x_{D,Hu} = (\dot{E}x_{21} + \dot{E}x_{23}) - (\dot{E}x_{24} + \dot{E}x_{22})$
Dehumidifier	$\dot{m}_{25} = \dot{m}_{23} (\omega_{24} - \omega_{23})$	$\dot{m}_{20} h_{20} + \dot{m}_{23} h_{23} + \dot{m}_{25} h_{25} = \dot{m}_{19} h_{19} + \dot{m}_{24} h_{24}$ $\varepsilon_{Dhu} = \max\left(\frac{(h_{23} - h_{24})}{(h_{23} - h_{24,ideal})}, \frac{(h_{20} - h_{19})}{(h_{20,ideal} - h_{19})}\right)$	$\dot{E}x_{D,Dhu} = (\dot{E}x_{24} + \dot{E}x_{19}) -$ $(\dot{E}x_{20} + \dot{E}x_{23} + \dot{E}x_{25})$

4.Model validation

Two valuable scenarios of the SOFC and HDH units are reckoned and simulated under similar conditions and results are juxtaposed with those of Ranjbar et al. [5] and Narayan et al. [17].

To substantiate the attained data of the current work, the alteration of current density with air compressor power, SOFC package work, and net electricity is sketched in Fig. 3. As this figure portrays, the current outcomes greatly concur with those of Ranjbar et al.[5].

Lastly, an HDH system is selected, modeled and the outcomes are juxtaposed with those of Narayan et al. [16] and the results are portrayed in Fig. 4. In this target, the minimum and maximum temperatures are presumed 303.15 K and 353.15 K, respectively. As comparison exhibits, the data of the current simulation in Fig. 4 utterly concurred with these scholars.

5.Results and discussion

Table 3 enumerated some preeminent thermodynamic parameters at each stream for the SOFC-GT-HDH system.

Table 4 outlines the outcomes of energetic and exergetic evaluation attained for the introduced set-up at the presumed input data of Table 1. As Table 6 portrays, the energetic and exergetic efficiencies of the hybrid system are accomplished at 81.87% and 55.26%, respectively. It discovered that the energetic efficiency of the fundamental system (SOFC system) is ameliorated from 53.88% to 56.76% for electricity. Also, adding a desalination unit has increased the energetic efficiency of the system to 81.87%. Thus, integrating the considered sub-systems into a monolithic system has indicated a satisfactory outline.

From an exergetic evaluation standpoint, the outcomes indicate that the exergetic efficiency of the SOFC stack increases as gas turbine and desalination units are added to the plant. On this basis, the exergetic efficiency is increased from 51.97% to 54.75% (approximately %), as the gas turbine is added to the SOFC set-up. Adding desalination units also increased exergetic efficiency up to 55.26%. Therefore, merging the desalination unit had a marginal influence on the overall system's efficiency from an exergy standpoint. Furthermore, the overall net electricity and distilled water rate are computed at 460.3 kW, and 307.368 kg/h, respectively. That 289.9 kW of it was obtained by the gas turbine..

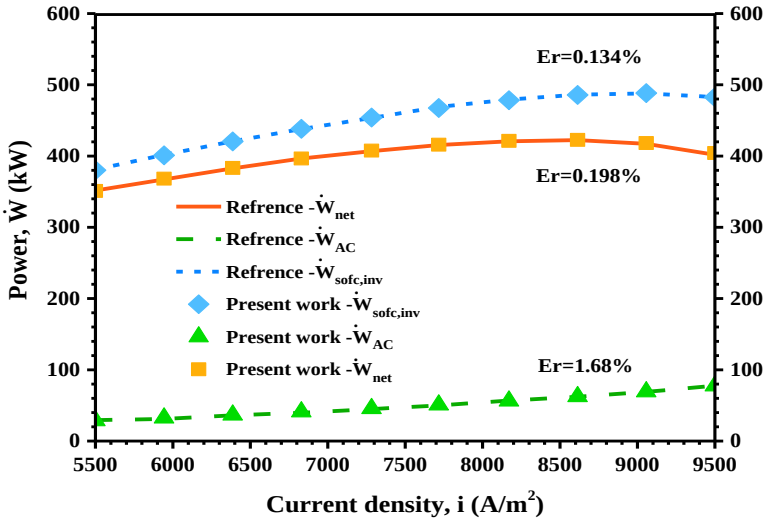

Fig. 3. Attained data of verification between the current study and Ranjbar et al. [5] for the SOFC system

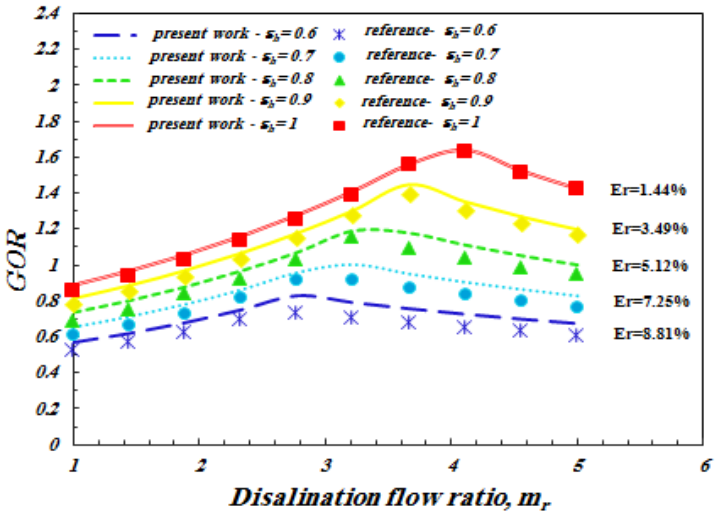

Fig.4: Attained data of verification between the current study and Narayan et al. [17] for the HDH system.

Table 3. Thermodynamic properties of the streams for the fuel cell part of the system.

State	T (K)	P (bar)	$\dot{m}$ (kg/s)	h (kJ/kg)	s $(kJ/kg.K)$	$E\dot{x}$ (kW)
1	298.2	1.013	0.9337	0	6.884	4.005
2	568.8	8.104	0.9337	278.3	6.947	246.2
3	860	7.942	0.9337	594.6	7.401	415.1
4	960	7.783	0.8836	709.7	7.535	460.5
5	298.2	1.013	0.01622	-4650	11.61	840.7
6	463.6	8.104	0.01622	-4236	11.63	847.3
7	860	7.942	0.01622	-2853	13.75	859.5
8	298.2	1.013	0.03643	104.8	0.3669	1.82
9	298.2	8.104	0.03643	105.7	0.3673	1.846
10	860	7.942	0.03643	3671	8.103	65.07
11	860	7.942	0.05264	-9385	12.58	902.6
12	960	7.783	0.1028	-9979	10.73	341.8
13	1137	7.55	0.9864	-415.7	8.136	743.6
14	1032	7.399	0.9864	-547.4	8.021	647.6
15	1014	7.251	0.9864	-570.1	8.005	630
16	766.9	7.106	0.9864	-869.5	7.673	432.3
17	510.4	1.043	0.9864	-1163	7.78	111
18	396.9	1.023	0.9864	-1288	7.509	35.89
19	298.2	1.013	2.71	99.77	0.3498	0
20	336.9	1.013	2.71	255	0.8393	25.1
21	348.2	1.013	2.71	300.4	0.9719	41.01
22	308.9	1.013	2.553	142.2	0.4891	1.837
23	304.4	1.013	1.129	98.77	5.951	0.2094
24	336.9	1.013	1.129	498.3	7.195	32.78
25	319.5	1.013	0.1574	194.1	0.6563	7.937

Figure 5 is sketched to portray the direct attribution of disparate constituents to the exergy destruction of the whole system. On the basis of this sketch, the heater, afterburner, and SOFC package are attributed to the highest exergy destruction by the amount of 61.22 kW, 58.75 kW, and 55.46 kW, respectively. By contrast, the pump and fuel compressor marginally attributed

to the overall loss by 0.00457 kW and 0.08833 kW, respectively.

Figure 6 sketched to portray shows the electricity and heating capacities of disparate constituents consumed or produced through the system's operation. In the manner of observation, the maximum electricity is produced by the solid oxide fuel cell (436.9 kW). The maximum capacity consumed in the system is in terms of heating and is in the third preheater by 295.3 kW, which is used for heating the input air into the fuel cell. This is obviously due to the high amount of air compared to other inlet fluids. In terms of electricity consumption, the air compression consumes around 259.8 kW of electricity to pressurize air, which is prominently due to the high rate of air intake compared to the other streams. As expected, the lowest electricity consumption is for pumps. The heat transfer capacity for the desalination heater is 130.5 kW and the heat transfer rate of preheaters 1 and 2 are attained at 129.9 kW and 22.42 kW, respectively.

Table 4. Performance parameters outcomes of the introduced polygeneration system.

Performance parameter	Value
Energetic efficiency of the hybrid system, $\eta_{en,tot}$ (%)	81.87
Net electrical energetic efficiency, $\eta_{en,elec}$ (%)	56.76
SOFC energetic efficiency, $\eta_{en,sofc}$ (%)	53.88
Exergetic efficiency of the hybrid system, $\eta_{ex,tot}$ (%)	55.26
Net electrical exergetic efficiency, $\eta_{ex,elec}$ (%)	54.75
Exergetic efficiency of SOFC, $\eta_{ex,sofc}$ (%)	51.97
Net electrical power, $\dot{W}_{net}$ (kW)	460.3
Net SOFC voltage, V (V)	0.7602
SOFC Power production, $\dot{W}_{inv,sofc}$ (kW)	436.9
Gas turbine power, $\dot{W}_{GT}$ (kW)	289.9
Distilled water rate, $\dot{m}_{dw}$ (kg/h)	307.368
GOR parameter for HDH cycle	1.56

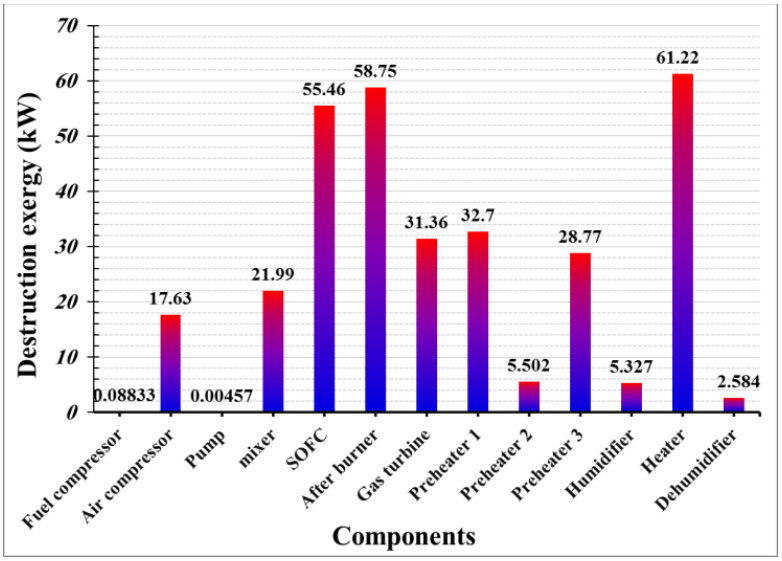

Fig.5: Exergy destruction rate for different components.

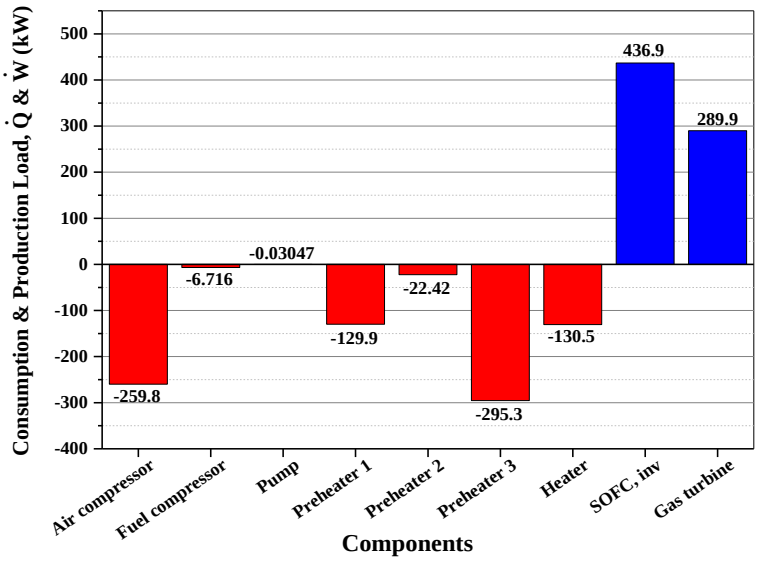

Fig.6: Electricity or heating consumption/production via disparate constituents.

6.Parametric study

This part investigates the impact of influential thermodynamic parameters, encompassing the SOFC temperature and current density, desalination flow ratio, HDH maximum temperature, and humidifier and dehumidifier effectivenesses on the critical thermodynamic performance factors.

6.1.Impact of SOFC current density on the main criteria of the hybrid system

Figure 7 is sketched to portray the alteration of net electricity generated by the overall system, distilled water rate at disparate current densities, and exergetic and energetic efficiencies. According to Fig. 7, increasing the current density engenders an increment in the amount of air, water, and fuel entering the cycle. As the flow rate increases, the required electricity to operate compressors and pumps will also increase subsequently. Increasing fuel means that more chemical energy is converted into electrical energy. The fuel cell electricity is directly related to the current density and voltage of the SOFC. However, considering the fact that since the current density is greater than the voltage, it will have a greater impact on the generated electricity and increases the electricity capacity of the SOFC. Raising the current density, as it was investigated, increases the demand for fuel, air, and water entering the cycle. Thus, according to the law of mass conservation, the gas rate at the outlet of the SOFC stack also augments, and hence more electricity will be extracted from the turbine. The amount of electricity produced by the SOFC stack and the gas turbine is substantial in comparison with the increment in electricity consumption. Therefore, changes in the net electricity with respect to the current density will be an uprising. Under a constant condition for the fuel cell, including fuel utilization factor and inlet temperature and temperature difference at its outlet, and due to small changes in the temperature of the flue gas as well, more heat is transferred to the desalination heater, engendering more seawater demand to the HDH system, resulting in more pure water production. By augmenting the current density of the fuel cell, as already mentioned, the amount of fuel entering the system raises. In other words, the energy and exergy amount of streams at the entering of the cycle increases. Also, increasing the current density intensifies the amount of net power and purified water but the influence of increment in required CH4 is more than and it thus decreases the total energetic and exergetic efficiency of the system.

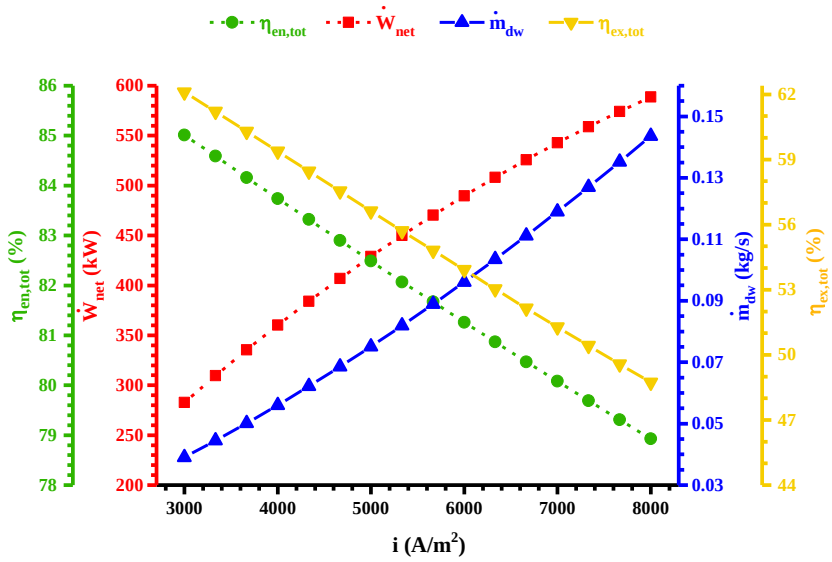

Fig .7. Impact of current density on the electricity, distilled water rate, energetic and exergetic efficiencies

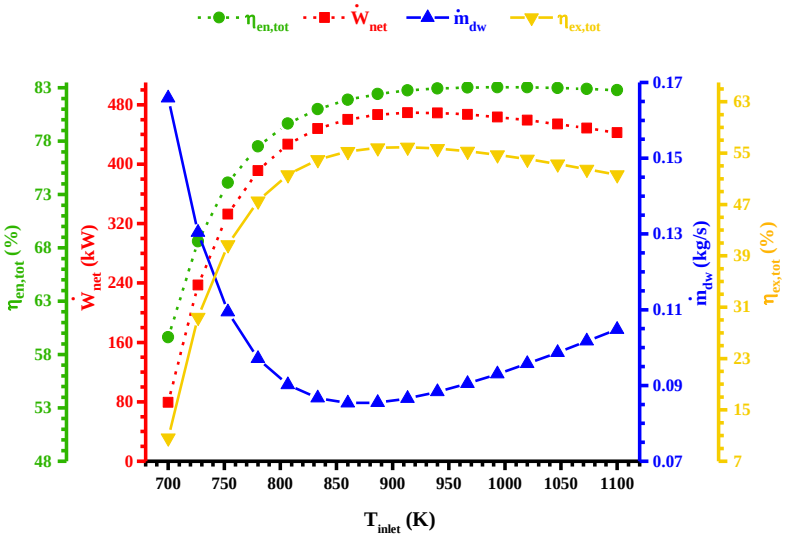

Fig.8: Impact of the SOFC inlet temperature on the electricity, distilled water rate, and energetic and exergetic efficiencies

6.2.Impact of SOFC inlet temperature on the main criteria of the hybrid system

Figure 8 portrays the effect of the SOFC temperature on the electricity, distilled water rate and energetic and exergetic efficiencies. As the SOFC inlet temperature increases, input CH_4 increases subtly, while the fuel cell lost voltage decreases, and hence the cell voltage increases. However, after the 860 K, the ohmic voltage is decreased as the SOFC inlet temperature increases, whilst the concentration and activation voltages are augmented; both approximately neutralize impacts of each other. Thus, a decrement of the Nernst voltage engenders a subtle decrement in the cell voltage, resulting in a maximum cell voltage at 860 K. Since cell voltage is directly proportional to the SOFC electricity, thus an acme will be observed for the SOFC electricity with respect to the

SOFC inlet temperature. Increasing the fuel cell inlet temperature will increase methane and water while reducing the air up to 860 K. Since the decrement rate of air is more substantial than the increment of methane and water, thus the gas turbine electricity will decline up to 860 K. After 860 K, the process is reversed and the gas turbine electricity increases onward. Additionally, decreasing air flow rate decreases the compressor consumption electricity substantially which gives a rise to the net electricity of the polygeneration system up to $T_{SOFC,in}$=860 K. However, the increment rate of the gas turbine electricity with increasing $T_{SOFC,in}$ is paramount than the decrement rate of the SOFC electricity, while the compressor consumption electricity does not decline from this point onward, culminating in subtle increment in net electricity from this point onward. According to Fig. 8, the distilled water rate declines as the SOFC inlet temperature increases up to 860 K and increases after that.

The maximum energetic and exergetic efficiencies of the system are about 83.6% and 55.93%, respectively, at 890 and 860 K which is proportional to the distilled water and directly extracted electricity from the fuel cell. Augmenting the fuel cell inlet temperature will give a rise to the net electricity up to 860 K with a steep slope, while the methane entering energy and exergy rates will also increase, and distilled water rate decreases. Since the increment rate of the net electricity is more substantial than that of the input methane, thus the energetic and exergetic efficiencies will increase up to that point and will remain almost constant from this point onwards, but the total exergetic efficiency of the whole system slowly decreases.

6.3.Impact of compression ratio on the main criteria of the hybrid system

Figure 9 depicts the alteration of electricity, distilled water, and energetic and exergetic efficiencies with disparate compression ratios. With increasing the SOFC stack pressure, the CH4 and water rates of the fuel cell remained constant, whilst the input air flow rate declined with a low slope. Increasing the SOFC stack pressure engenders a minor rise in the voltage and a low decrease in the loss voltage. Thus, the cell voltage will Increase slightly with any increment in the compression ratio, culminating in subtle augmentation of SOFC electricity. Meantime, increasing the compression ratio engenders a drop in the flow rate of the intake air, decreasing the flow rate of individual hot flue gases. Also, with the constant SOFC temperature and constant temperature difference entrance and exit of SOFC, it is discovered that the enthalpy difference through the turbine is skyrocketed with increasing the compression ratio which is more appreciable than the decrement of flue gas flow rate, and hence the gas turbine extracted electricity will rise. All in all, the net electricity of the hybrid system will augment by raising the compression ratio since the consumption electricity of compressors is also decreased (due to a decrease in the airflow rate). A decrease in the flow rate of flue gas also supplies less heat to the HDH system, and hence less distilled water will be extracted as well.

On the basis of Fig. 9, due to the small value of the effect of distilled water on efficiency, the total efficiency (both energetic and exergetic efficiencies) is augmented as compression ratio rises since the SOFC stack and gas turbine generated more electricity.

Figure 10 portrays changes in the desalination flow ratio with GOR, distilled water rate, energetic efficiency, and exergetic efficiency. In pursuance of this goal, the desalination flow ratio has been changed from 0.5 to 6. As can be seen (and argued in the validation section of the HDH system), an increase in the desalination flow ratio in values below 2.4 results in an increase in the GOR up to 1.56 and distilled water by 0.0848 kg/s. From a ratio of 2.4 onward, the GOR and distilled water rate will be reduced in parallel. This tendency will alter the energetic and exergetic efficiencies of the whole system in the same configuration as well.

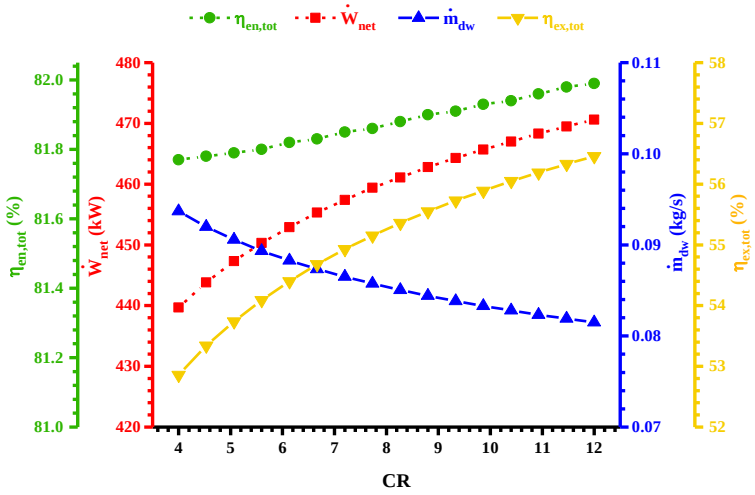

Fig.9: Impact of compression ratio on the electricity, distilled water rate, energetic and exergetic efficiencies.

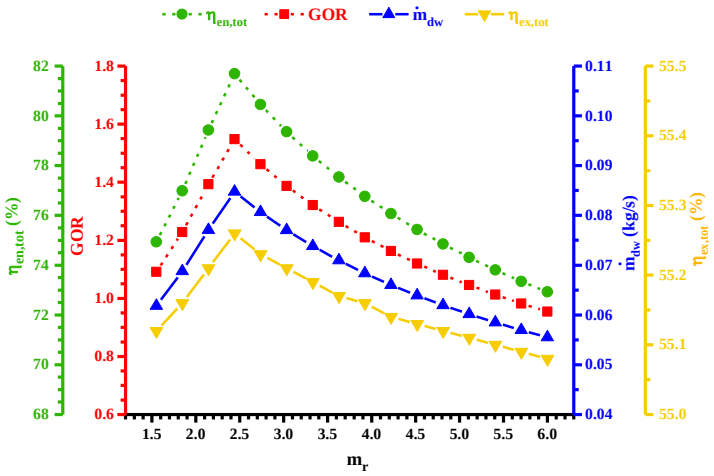

Fig.10: Impact of desalination flow ratio on the GOR, distilled water rate, and energetic and exergetic efficiencies.

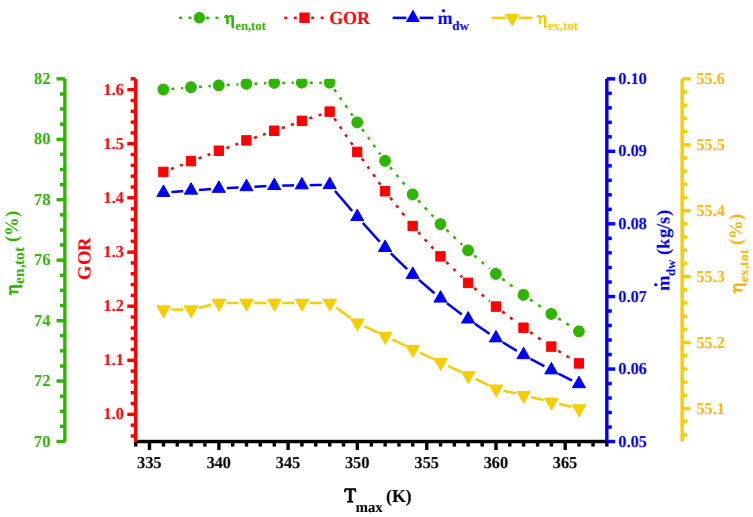

Fig.11: Impact of desalination maximum temperature on the GOR, distilled water rate, and energetic and exergetic efficiencies.

6.4. Impact of desalination maximum temperature on the main criteria of the hybrid system

Figure 11 shows the alteration in the GOR, distilled water rate, energetic efficiency, and exergetic efficiency with disparate desalination maximum temperatures. As can be seen, the changes in the GOR up to a maximum temperature of 347.9 K are uplifting, whilst declines after this point. Until this temperature, the amount of distilled water is unvaried with the maximum temperature (very slightly increases) and declines after $T_{Max,HDH}$ =347.9 K. However, the input heat of the desalination system decreases as the $T_{Max,HDH}$ augments. Thus, decrement in the input heat prior to the point of $T_{Max,HDH}$ =347.9 K affects the GOR downwardly, while the substantial decline of distilled water after this point influences the GOR, and thus the GOR declines thereafter. The trend of changes in energetic and exegetic efficiencies follow the alteration of distilled water rate, as substantiated by this figure.

7. Conclusion

A new hybrid set-up is reckoned and evaluated on the basis of thermodynamics laws. An extensive thermodynamic and parametric evaluation of the introduced set-up is tendered to portray the impact of some main thermodynamic input data on the central factors. The expanded mathematical model was testified by accessible experimental and theoretical data. The following conclusions are tendered:

- Amongst all elements, the heater, afterburner and SOFC stack were recognized as the utmost destructive constituents by 61.22 kW, 58.75 and 55.46 kW, correspondingly.
- The reckoned hybrid set-up generated electricity, and distilled water of 460.3 kW, and 307.368 kg/h, respectively. Regarding that, the overall system's energetic and exergetic efficiencies were computed at 81.87% and 55.26%, respectively.
- Higher energetic and exergetic efficiencies were attained by a decrement in the current density and increment in compression ratio, $T_{sofc,in}$ and $T_{max,HDH}$ until 860 K and 347.9 K, respectively.

The main factors of the integrated system are introduced and the impact of their changes on system performance and products are investigated.

References

[1] Jia, J., et al., Performance comparison of three solid oxide fuel cell power systems. International Journal of Energy Research, 2013. 37(14): p. 1821-1830.

[2] Ghaebi, H., A.S. Namin, and H. Rostamzadeh, Performance assessment and optimization of a novel multi-generation system from thermodynamic and thermoeconomic viewpoints. Energy Conversion and Management, 2018. 165: p. 419-439.

[3] Behzadi, A., et al., Multi-objective optimization of a hybrid biomass-based SOFC/GT/double effect absorption chiller/RO desalination system with CO2 recycle. Energy conversion and management, 2019. 181: p. 302-318.

[4] Gholamian, E. and V. Zare, A comparative thermodynamic investigation with environmental analysis of SOFC waste heat to power conversion employing Kalina and Organic Rankine Cycles. Energy Conversion and Management, 2016. 117: p. 150-161.

[5] Ranjbar, F., et al., Energy and exergy assessments of a novel trigeneration system based on a solid oxide fuel cell. Energy Conversion and Management, 2014. 87: p. 318-327.

[6] Chitsaz, A., A. Mehr, and S. Mahmoudi, Exergoeconomic analysis of a trigeneration system driven by a solid oxide fuel cell. Energy Conversion and Management, 2015. 106: p. 921-931.

[7] Chitsaz, A., J. Hosseinpour, and M. Assadi, Effect of recycling on the thermodynamic and thermoeconomic performances of SOFC based on trigeneration systems; A comparative study. Energy, 2017. 124: p. 613-624.

[8] Hosseinpour, J., et al., Investigation on performance of an integrated SOFC-Goswami system using wood gasification. Energy, 2018. 148: p. 614-628.

[9] Al-Sulaiman, F.A., F. Hamdullahpur, and I. Dincer, Performance comparison of three

trigeneration systems using organic Rankine cycles. Energy, 2011. 36(9): p. 5741-5754.

[10] Yari, M., et al., A comparative study of two SOFC-based cogeneration systems fed by municipal solid waste by means of either the gasifier or digester. Energy, 2016. 114: p. 586-602.

[11] Hosseini, M., et al., Thermodynamic modelling of an integrated solid oxide fuel cell and micro gas turbine system for desalination purposes. International Journal of Energy Research, 2013. 37(5): p. 426-434.

[12] Sattari Sadat, S.M. and H. Ghaebi, Design and evaluation of a novel SOFC-driven multi-generation system. Journal of Energy Management and Technology, 2019. 3(4): p. 25-41.

[13] Ma, S., et al., Thermodynamic analysis of a new combined cooling, heat and power system driven by solid oxide fuel cell based on ammonia–water mixture. Journal of Power Sources, 2011. 196(20): p. 8463-8471.

[14] Chan, S., C. Low, and O. Ding, Energy and exergy analysis of simple solid-oxide fuel-cell power systems. Journal of Power Sources, 2002. 103(2): p. 188-200.

[15] Kim, J.W., et al., Polarization effects in intermediate temperature, anode-supported solid oxide fuel cells. Journal of the Electrochemical Society, 1999. 146(1): p. 69-78.

[16] Bossel, U., Final report on SOFC Data Facts & Figures Swiss Federal Office of Energy. 1992.

[17]Narayan, G.P., et al., Thermodynamic analysis of humidification dehumidification desalination cycles. Desalination and water treatment, 2010. 16(1-3): p. 339-353.

[18] Narayan, G.P., R.K. McGovern, and S.M. Zubair, High-temperature-steam-driven, varied-pressure, humidification-dehumidification system coupled with reverse osmosis for energy-efficient seawater desalination. Energy, 2012. 37(1): p. 482-493.

[19] Narayan, G.P., et al., Thermal design of the humidification dehumidification desalination system: An experimental investigation. International Journal of Heat and Mass Transfer, 2013. 58(1): p. 740-748.

[20] Bejan, A. and G. Tsatsaronis, Thermal design and optimization. 1996: John Wiley & Sons.

[21] Wang, J., et al., Thermodynamic analysis of an integrated power generation system driven by solid oxide fuel cell. International Journal of Hydrogen Energy, 2012. 37(3): p. 2535-2545.

[22] Colpan, C.O., I. Dincer, and F. Hamdullahpur, Thermodynamic modeling of direct internal reforming solid oxide fuel cells operating with syngas. International Journal of Hydrogen Energy, 2007. 32(7): p. 787-795.

[23] Sharqawy, M.H., et al., Optimum thermal design of humidification dehumidification desalination systems. Desalination, 2014. 349: p. 10-21.